analytical chemistry

pubs.acs.org/ac

Article

Hydrophobic Localized Enrichment of Co-reactants to Enhance Electrochemiluminescence of Conjugated Polymers for Detecting SARS-CoV-2 Nucleocapsid Proteins

Yingying Chen, Ying He, Jinwen Zhao, Jin Zhang, Ruo Yuan, and Shihong Chen*

Cite This: *Anal. Chem.* 2022, 94, 4446−4454

Read Online

ACCESS | Metrics & More | Article Recommendations | Supporting Information

ABSTRACT: The enrichment of co-reactants is one of the keys to improving the sensitivity of electrochemiluminescence (ECL) detection. This work developed a novel hydrophobic localized enrichment strategy of co-reactants utilizing the inner hydrophobic cavity of β-cyclodextrin (β-CD). Pt nanoparticles (Pt NPs) were grown in situ on the coordination sites for metal ions of β-CD to prepare the β-CD-Pt nanocomposite, which could not only enrich co-reactant 3-(dibutylamino) propylamine (TDBA) highly efficiently through its hydrophobic cavity but also immobilize TDBA via the Pt−N bond. Meanwhile, the carboxyl-functionalized poly[2,5-dioctyl-1,4-phenylene] (PDP) polymer nanoparticles (PNPs) were developed as excellent ECL luminophores. With SARS-CoV-2 nucleocapsid protein (ncovNP) as a model protein, the TDBA-β-CD-Pt nanocomposite combined PDP PNPs to construct a biosensor for ncovNP determination. The PDP PNPs were modified onto the surface of a glassy carbon electrode (GCE) to capture the first antibody (Ab_1) and further capture antigen and secondary antibody complexes (TDBA-β-CD-Pt@Ab_2). The resultant biosensor with a sandwich structure achieved a highly sensitive detection of ncovNP with a detection limit of 22 fg/mL. TDBA-β-CD-Pt shared with an inspiration in hydrophobic localized enrichment of co-reactants for improving the sensitivity of ECL detection. The luminophore PDP PNPs integrated TDBA-β-CD-Pt to provide a promising and sensitive ECL platform, offering a new method for ncovNP detection.

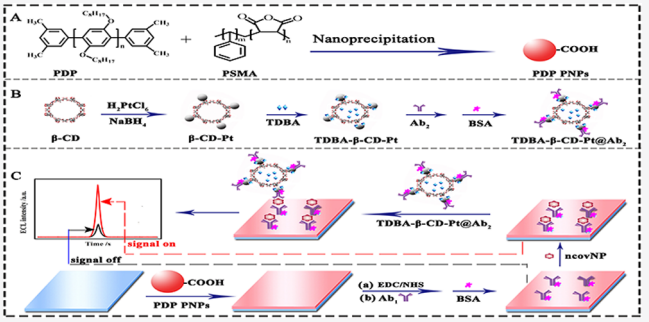

INTRODUCTION

Severe acute respiratory syndrome coronavirus 2 (SARS-CoV-2) has caused many deaths worldwide.[1] As one of the four major structural proteins of SARS-CoV-2, the nucleocapsid protein (NP) with the most abundant structural features was generally considered as a biomarker of SARS-CoV-2.[2] Recently, several methods have been developed to detect the SARS-CoV-2 nucleocapsid protein (ncovNP), such as enzyme-linked immunosorbent assays (ELISAs),[3] luciferase IP system (LIPS),[4] and lateral flow assay (LFA).[5] However, those reported methods were characterized by a low sensitivity or complex operation, so their applications were limited.[6] The development of a sensitive and simple test for ncovNP is critical.

Electrochemiluminescence (ECL) technology is characterized by low background, high sensitivity, and simple operation and has attracted extensive attention in clinical analysis, environmental monitoring, and food safety.[7,8] The nucleic acid detection related to SARS-CoV-2 using the ECL method has been reported.[9] The sensitivity of nucleic acid detection is relatively high, but it has disadvantages such as cumbersome extraction process and false-negative results.[10] Compared with nucleic acid detection, protein detection is characterized by a simpler operation, higher specificity, and higher accuracy.[11] So far, there are few reports concerning the ECL protein detection of ncovNP. Thus, ECL strategies for ncovNP protein detection are worth exploring.

An excellent ECL luminophore is one of the keys to achieving highly sensitive ECL detection. Among the numerous ECL luminophores such as organic polymers, inorganic complex, organic small molecules, and inorganic nanomaterials such as metal nanoclusters and various quantum dots, the organic polymers have received great attention due to their high photostability, low cellular toxicity, and easy functionalization.[12,13] The organic polymers reported as ECL signal probes mainly include polyfluorene and polyfluorene derivatives, poly(phenylenevinylene), and heterocycle-containing polymers. For example, the polyfluorene derivatives PFBT[13] and PFO[14] were developed as ECL luminophores to

Received: December 14, 2021
Accepted: February 21, 2022
Published: March 1, 2022

https://doi.org/10.1021/acs.analchem.1c05407
Anal. Chem. 2022, 94, 4446−4454

Scheme 1. Preparation of (A) PDP PNPs and (B) TDBA-β-CD-Pt@Ab_2. (C) Illustration of the Construction of Biosensor for ncovNP Determination.

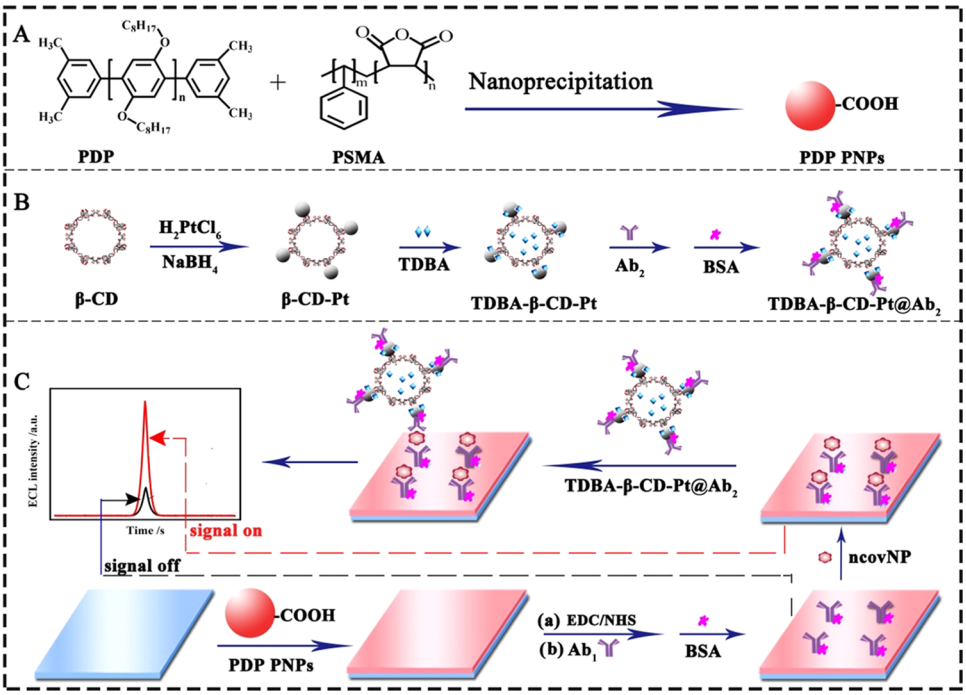

achieve true-color ECL imaging for detecting multiplex and ratio detection of microRNA-155, respectively. Cui's group used heterocycle-containing thiophene-fused conjugated microporous polymer with a strong dual-band bipolar ECL emission to detect rhodamine B.[15] Ju's group prepared polymer dots containing poly(phenylenevinylene) CN-PPV with high ECL efficiency to construct an ECL biosensor for detecting Fe^{3+}.[16] The types of organic polymer reported in the literature are limited. It is significant to develop new ECL polymer luminophores.

The introduction of co-reactants is also crucial for highly sensitive ECL detection. The most common method to introduce co-reactants is to add them directly into the detection solution. Such a method is simple, but the stability and repeatability problems of the ECL system cannot be ignored.[17] The in situ production of co-reactants by the enzyme-catalyzed reaction faces complex operation and harsh conditions of enzyme use, so its applications are limited.[18] Attaching co-reactants to the electrode surface can overcome the disadvantage of introducing the co-reactants described above, and some strategies such as covalent bonding and cross-linking have been adopted.[19,20] However, it is still challenging to achieve high loading of co-reactants on the electrode surface. Since the hydrophobic localized enrichment can significantly enhance the concentration of co-reactants on the electrode surface, enriching co-reactants by the material with a hydrophobic cavity may be an ideal choice to realize high loading of co-reactants on the electrode surface. For example, Yuan's group synthesized hydrophobic porous covalent organic frameworks (COFs) as microreactors to provide co-reactants with the microenvironment, thus achieving a confinement-enhanced ECL.[21] Yuan's group also reported that the co-reactants could be enriched around the electrode surface by hydrophobic interaction between cholesterol and co-reactants.[22] However, the hydrophobic localized enrichment of co-reactants described above was for the co-reactants present in the detection solution, which still caused stability and repeatability problems in the ECL system.[17] Therefore, it is of great value to develop a material with an inner hydrophobic cavity for enriching co-reactants to achieve their immobilization on the electrode surface.

β-Cyclodextrin (β-CD) has an inner hydrophobic cavity and an outer large number of the hydroxyl groups and has been widely used for functionalization of materials, guest recognition, and coordination with metal ions in the ECL field. For example, Chen's group applied β-CD-functionalized carbon nanohorns to detect naringin based on the fact that naringin could enter into the cavity of β-CD to form an inclusion complex.[23] He's group utilized the host–guest recognition between aptamer and tris(bipyridine)ruthenium(II)-β-cyclodextrin for detecting thrombin.[24] Wei's group utilized metal-binding sites of β-CD to bind Pb^{2+} for synthesizing metal–organic frameworks (MOFs).[25] In addition, the hydrophobic nanocavity of β-CD could act as a nanoreactor, creating a restricted system to accelerate electronic excitation.[26] The restriction effect of nanocavity and binding sites with metal ions of β-CD may provide two completely different forces for simultaneously immobilizing co-reactants, namely, hydrophobic localized enrichment and covalent bonding through metal nanoparticles grown in situ on β-CD.

Inspired by the above observations, this work developed a simple and effective strategy for hydrophobic localized enrichment of co-reactant 3-(dibutylamino) propylamine (TDBA) utilizing the inner hydrophobic cavity of β-CD. On the other hand, the coordination sites for metal ions of β-CD make it easy for Pt nanoparticles (Pt NPs) to grow in situ on β-CD, which could immobilize TDBA and the second antibody (Ab_2) via the Pt–N bond. Meanwhile, the carboxyl-functionalized poly[2,5-dioctyl-1,4-phenylene] polymer nanoparticles (PDP PNPs) were developed as luminophores. As seen from its molecular structure in Scheme 1, obviously, PDP is different from other reported ECL organic

https://doi.org/10.1021/acs.analchem.1c05407
Anal. Chem. 2022, 94, 4446–4454

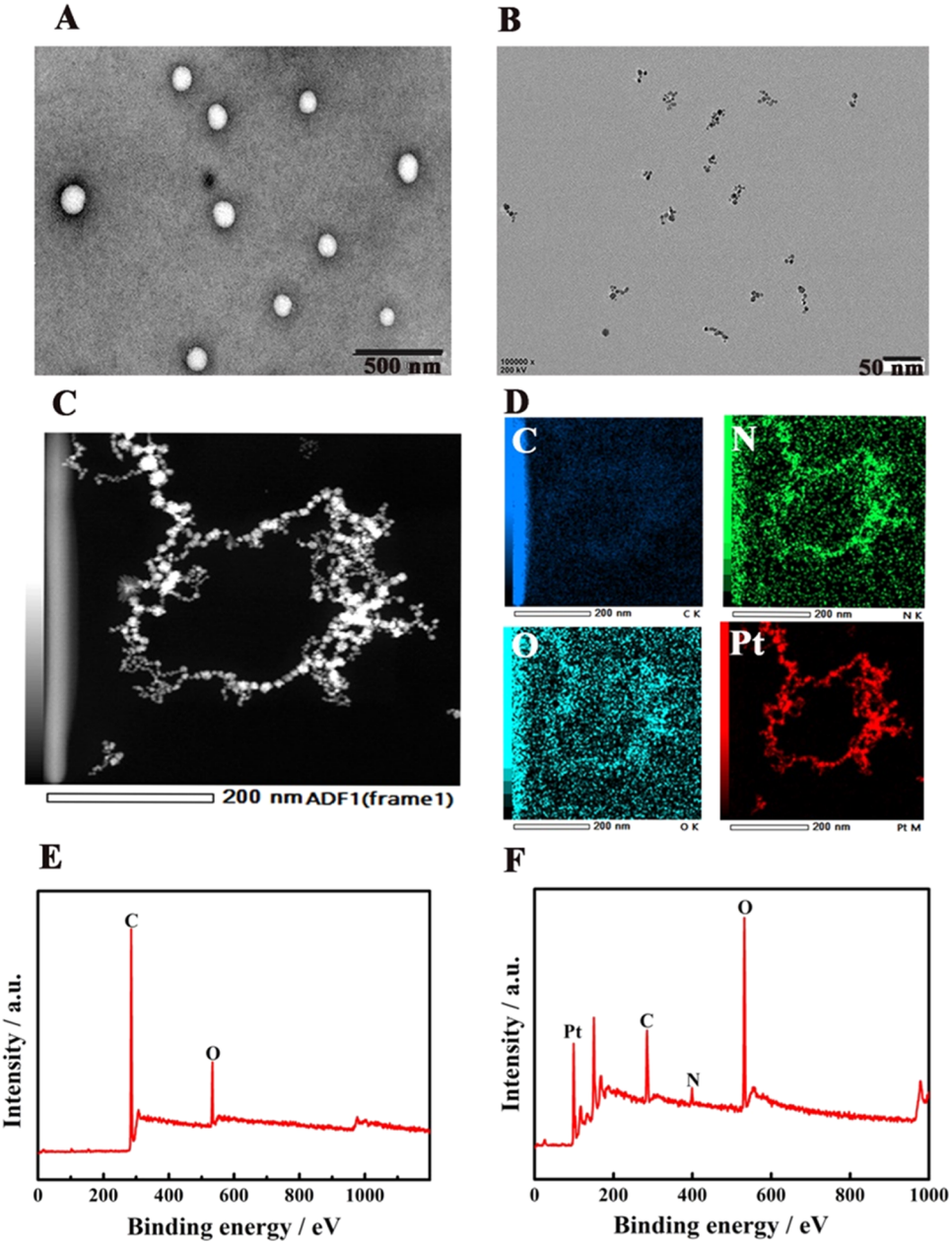

Figure 1. (A) TEM images of PDP PNPs. (B) SEM images of Pt NPs. (C) TEM images of β-CD-Pt and (D) the corresponding elemental mapping of C, N, O, and Pt. XPS spectra of (E) PDP PNPs and (F) β-CD-Pt.

polymers, including polyfluorene derivatives, poly(phenylenevinylene), and heterocycle-containing polymers, and is a kind of biphenyl polymer with a relatively simple structure. PDP PNPs have good dispersibility and stability in water, as well as excellent luminescence stability. PDP PNPs were modified onto the GCE surface to capture the first antibody (Ab_1) and further capture ncovNP and the secondary antibody complex (TDBA-β-CD-Pt@Ab_2). Due to the systematic action of hydrophobic localized enrichment and covalent bonding, the amount of TDBA immobilized on the electrode surface was increased significantly, and the ECL intensity was improved nearly fivefold as compared to that without β-CD, thus achieving a sensitive detection of ncovNP with a detection limit of 22 fg/mL. β-CD provided an attractive strategy for high loading co-reactants on the electrode surface. The integration of β-CD-Pt nanocomposites as excellent carriers of co-reactants and PDP PNPs as an excellent ECL luminophore would build an attractive ECL platform and shed light on the ultrasensitive detection of ncovNP.

EXPERIMENT SECTION

Preparation of PDP PNPs. First, tetrahydrofuran (THF) was applied to dissolve 5.0 mg of PDP and 1.0 mg of PSMA to make their respective solutions (1.0 mg/mL). Subsequently, the obtained PDP and PSMA solutions were sufficiently mixed for 2.0 h and further injected into deionized water (10 mL). Next, the resultant mixed solution was heated under an air atmosphere at 80 °C until THF was completely evaporated to obtain a PDP PNP dispersion. Scheme 1A plots the preparation procedure of PDP PNPs.

Preparation of the β-CD-Pt Nanocomposite. Briefly, 1.0 mg of β-CD was dissolved in deionized water with vigorous

https://doi.org/10.1021/acs.analchem.1c05407
Anal. Chem. 2022, 94, 4446−4454

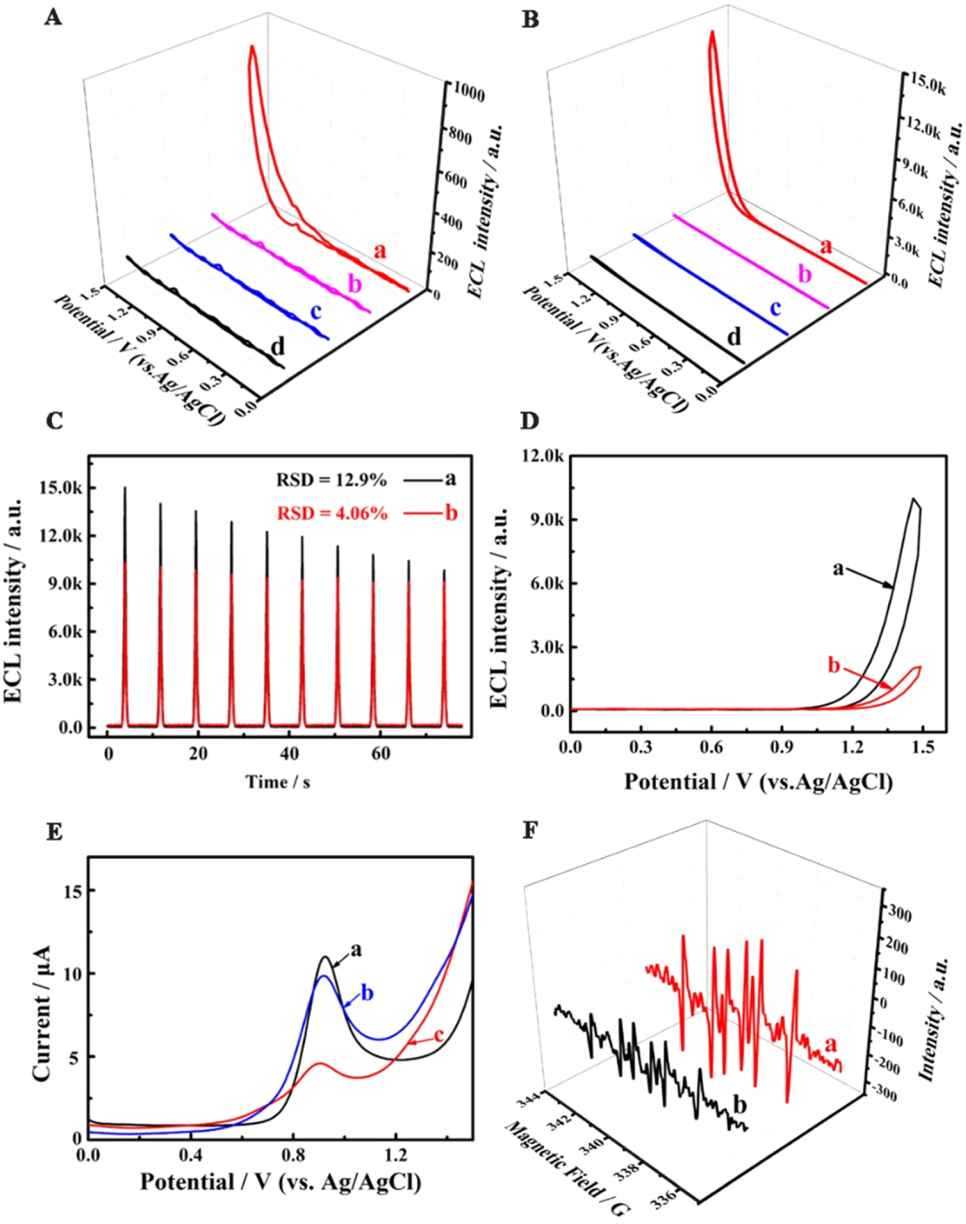

Figure 2. (A) ECL responses of differently modified electrodes (A) without and (B) with 5.7 mM TDBA: (a) PDP PNPs/GCE, (b) β-CD-Pt/GCE, (c) β-CD/GCE, and (d) Pt NPs/GCE. (C) ECL stability of (a) PDP PNPs/GCE with 5.7 mM TDBA and (b) TDBA-Pt@Ab_2/ncovNP/Ab_1/PDP PNPs/GCE. (D) ECL signals of (a) TDBA-β-CD-Pt@Ab_2/ncovNP/Ab_1/PDP PNPs/GCE and (b) TDBA-Pt@Ab_2/ncovNP/Ab_1/PDP PNPs/GCE. (E) Anodic DPV profiles of (a) bare GCE with 5.7 mM TDBA, (b) TDBA-β-CD-Pt@Ab_2/ncovNP/Ab_1/PDP PNPs/GCE, and (c) TDBA-Pt@Ab_2/ncovNP/Ab_1/PDP PNPs/GCE. (F) EPR spectra of (a) TDBA-β-CD-Pt and (b) TDBA-Pt under light irradiation. Detection solution of PBS (3.0 mL, 0.10 M, pH 7.4) and the scanning rate of 300 mV/s for ECL and 100 mV/s for DPV.

sonication to form 1.0 mg/mL β-CD solution. Then, 10 μL of H_2PtCl_6 (1%) was added to the β-CD solution and the mixture was intensely stirred overnight. Thereafter, 25 μL of $NaBH_4$ (0.01 M) was slowly added into the above mixed solution to react for 20 min under stirring. Then, 10 μL of sodium citrate (0.01 M) was added and the mixture was continuously stirred for 30 min to form the β-CD-Pt nanocomposite, which was collected by centrifuging at 10 000 rpm and washing with water three times. Finally, the collected β-CD-Pt was dispersed in 1.0 mL of water to obtain its dispersion.

As a control, the Pt nanoparticles (Pt NPs) were prepared according to the above reduction method in the absence of β-CD.

Preparation of the TDBA-β-CD-Pt@Ab_2 Composite. The preparation procedure of the secondary antibody complex (TDBA-β-CD-Pt@Ab_2) is depicted in Scheme 1B. Briefly, 4.0 μL of TDBA, 400 μL of β-CD-Pt dispersion, and 40 μL of Ab_2 (50 μg/mL) were mixed and reacted under 4.0 °C for 14 h to form the TDBA-β-CD-Pt@Ab_2 nanocomposite. Then, the remaining active sites of TDBA-β-CD-Pt@Ab_2 were blocked by incubating BSA (1%, 100 μL) with the nanocomposite for 40 min. Finally, the resultant TDBA-β-CD-Pt@Ab_2 was centrifuged at 8000 rpm and washed three times using 0.10 M PBS (pH 7.4) and further dispersed in 400 μL of 0.10 M PBS (pH 7.4). The obtained product was stored at 4.0 °C for later use.

https://doi.org/10.1021/acs.analchem.1c05407
Anal. Chem. 2022, 94, 4446−4454

Fabrication of the ECL Immunosensor. After being polished with alumina (0.3 and 0.05 μm) and ultrasonically cleaned alternately using pure water and ethanol, the GCE (Φ = 4.0 mm) was covered with the PDP PNP dispersion (10 μL) and naturally dried at room temperature. Then, the carboxyl groups of PDP PNPs were activated by incubating the electrode with EDC/NHS (v/v 4:1, 10 μL) for 1.0 h at room temperature. Hereafter, the first antibody (Ab_1, 10 μL) was incubated on the modified electrode for 14 h at 4.0 °C. Then, BSA (1%, 10 μL) was further incubated on a modified electrode for 1.0 h to block remnant binding sites of PDP PNPs to obtain the ECL immunosensor (Ab_1/PDP PNPs/GCE). PBS (0.10 M, pH 7.4) was used to wash the electrodes in each modification step. The preparation process is depicted in Scheme 1C.

ECL Measurement. The immunosensor (Ab_1/PDP PNPs/GCE) was incubated with different concentrations of ncovNP at 37 °C for 1.0 h, and then the TDBA-β-CD-Pt@Ab_2 bioconjugate was captured by incubating it on the electrode surface at 37 °C for 1.0 h to construct a sandwich structure. The modified GCE as a working electrode, platinum wire as a counter electrode, and an Ag/AgCl reference electrode formed a three-electrode system to record the ECL signals. The ECL detection was performed in 0.10 M of PBS (3.0 mL, pH 7.4). The scanning potential was from 0 V to +1.5 V and the scanning rate and the photomultiplier tube (PMT) were set to 300 mV/s and 800 V, respectively.

RESULTS AND DISCUSSION

Morphologies and Element Characterization of Nanomaterials. The scanning electron microscopy (SEM) and transmission electron microscopy (TEM) images of the prepared nanomaterials were recorded to observe their morphologies. Figure 1A depicts the TEM images of PDP PNPs, which exhibit a spherical shape with an average diameter of 103 nm. Figure 1B shows the SEM images of Pt NPs, which reveal the dissociative Pt NPs with an average size of about 30 nm. Figure 1C is the TEM images of the β-CD-Pt nanocomposite and shows a large number of Pt NPs. The assembly and arrangement of Pt NPs clearly revealed the cavity structure of the circinate shape of β-CD, indicating that Pt NPs were grown in situ on the coordination sites for the metal ions of β-CD. Moreover, the energy-dispersive scanning (EDS) mapping was employed to ensure the elemental distribution of β-CD-Pt. Figure 1D displays the EDS mapping of C, N, O, and Pt elements. It was demonstrated that Pt NPs were assembled on the β-CD molecules.

X-ray photoelectron spectroscopy (XPS) of PDP PNPs and β-CD-Pt was explored to further ensure their element distribution. Figure 1E clearly depicts the characteristic peaks of C 1s and O 1s from PDP PNPs. The corresponding XPS spectrum of each element with various bonds is shown in Figure S1A,B, respectively. As seen, the binding energies of C−C, C−O, and C═O of C 1s are 284.88, 286.29, and 287.6 eV, respectively (Figure S1A), and the binding energies of C−O and C═O in O 1s are 532.49 and 533.68 eV, respectively (Figure S1B). The existence of the C═O covalent bond indicates that PDP PNPs were successfully functionalized with carboxyl groups. Figure 1F depicts the XPS characteristic peaks of C, O, N, and Pt elements in β-CD-Pt. The corresponding bonding characteristic peaks of N 1s and Pt 4f are displayed in Figure S1C,D, respectively. The binding energies of Pt−N, C−N, and N−H in N 1s are found to be 398.28, 399.56, and 401.37 eV, respectively (Figure S1C), and the binding energies of Pt−N $4f_{7/2}$ and Pt−N $4f_{5/2}$ can be observed to be 72.53 and 76.5 eV, respectively (Figure S1D). The XPS characteristic peaks from β-CD-Pt demonstrate the successful preparation of β-CD-Pt.

In addition, the preparation of PDP PNPs was further characterized by Fourier transform-infrared (FT-IR) and ultraviolet−visible (UV−vis) absorption spectra, and the corresponding results are shown in Figure S2A,B in the Supporting Information, respectively. Meanwhile, the fluorescence (FL) excitation wavelength, the emission wavelength, and the ECL spectrum of PDP PNPs were explored, and the results are depicted in Figure S2C. Figure S2D displays the three-dimensional surface image of ECL from PDP PNPs. See the Supporting Information for the detailed discussion concerning Figure S2A−D. The FT-IR, UV−vis absorption, and FL spectrum results further demonstrate the successful preparation of PDP PNPs. The dispersibility in water and luminescence stability of PDP PNPs were also explored, and Figure S3 depicts the results. The detailed discussion is presented in the Supporting Information.

ECL Mechanism. The ECL behaviors of different materials including PDP PNPs, β-CD-Pt, β-CD, and Pt NPs were investigated using their corresponding modified electrodes in 0.10 M PBS (pH 7.4). Figure 2A,B depicts the ECL signals without and with 5.7 mM TDBA in PBS, respectively. As seen, whether or not co-reactant TDBA was present, almost no ECL signals were detected at β-CD-Pt/GCE (curve b), β-CD/GCE (curve c), and Pt NPs/GCE (curve d). However, the PDP PNPs/GCE exhibited a weak ECL signal (Figure 2A, curve a) in the absence of TDBA and a strong ECL response at +1.5 V in the presence of TDBA (Figure 2B, curve a), indicating that the detected ECL emission originated from PDP PNPs, not β-CD or Pt NPs. Moreover, it was also revealed that TDBA can act as a co-reactant to enhance the ECL signal of PDP PNPs. Meanwhile, the effect of PSMA on the ECL signal of the prepared PDP PNPs was confirmed by comparing the ECL responses of PDP nanoparticles with and without PSMA, and the corresponding descriptions are presented in the Supporting Information and the results are given in Figure S4.

We compared the stability of ECL signals with the co-reactant TDBA added to the detection solution and immobilized onto the electrode surface. Figure 2C depicts the corresponding results. For TDBA (5.7 mM) in PBS, the ECL signals under successive potential scanning for 10 cycles were recorded at PDP PNPs/GCE, and the results are plotted in Figure 2C (curve a). When TDBA was immobilized on the GCE, the ECL signal was detected at the biosensor TDBA-β-CD-Pt@Ab2/ncovNP/Ab_1/PDP PNPs/GCE. The results are presented in Figure 2C (curve b). As observed, curve a shows decreasing ECL signals as the number of cyclic scans increases and the relative standard deviation (RSD) is 12.9%. However, curve b shows a stable ECL emission under the same number of cyclic scans, and the corresponding RSD was 4.06%, which revealed the superiority of immobilizing TDBA onto the electrode by the β-CD-Pt nanocomposite.

The amplification effect of β-CD on the ECL emission of PDP PNPs was further explored. As a comparison, TDBA-Pt@Ab_2/ncovNP/Ab_1/PDP PNPs/GCE without β-CD was also constructed using the same assembly method as the biosensor (TDBA-β-CD-Pt@Ab_2/ncovNP/Ab_1/PDP PNPs/GCE) by substituting TDBA-Pt for TDBA-β-CD-Pt. As seen from Figure 2D, the ECL signal strength without β-CD was about

https://doi.org/10.1021/acs.analchem.1c05407
Anal. Chem. 2022, 94, 4446−4454

Scheme 2. ECL Mechanisms of PDP PNPs/TDBA System without and with β-CD

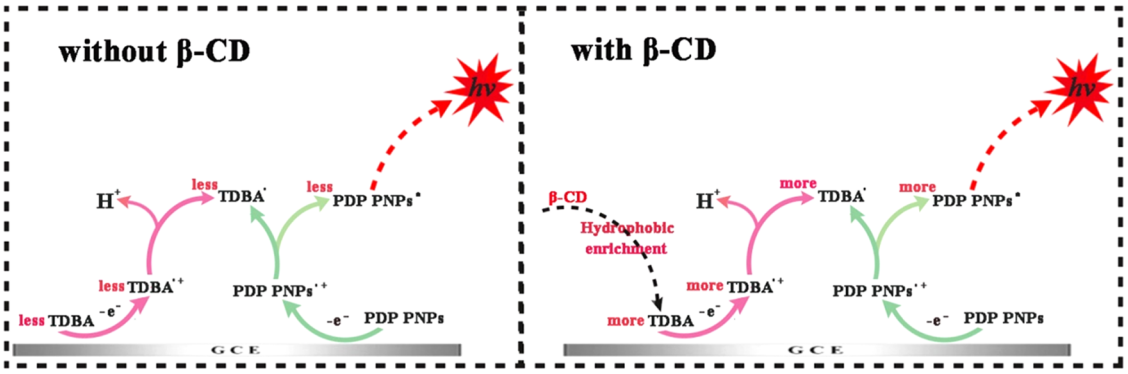

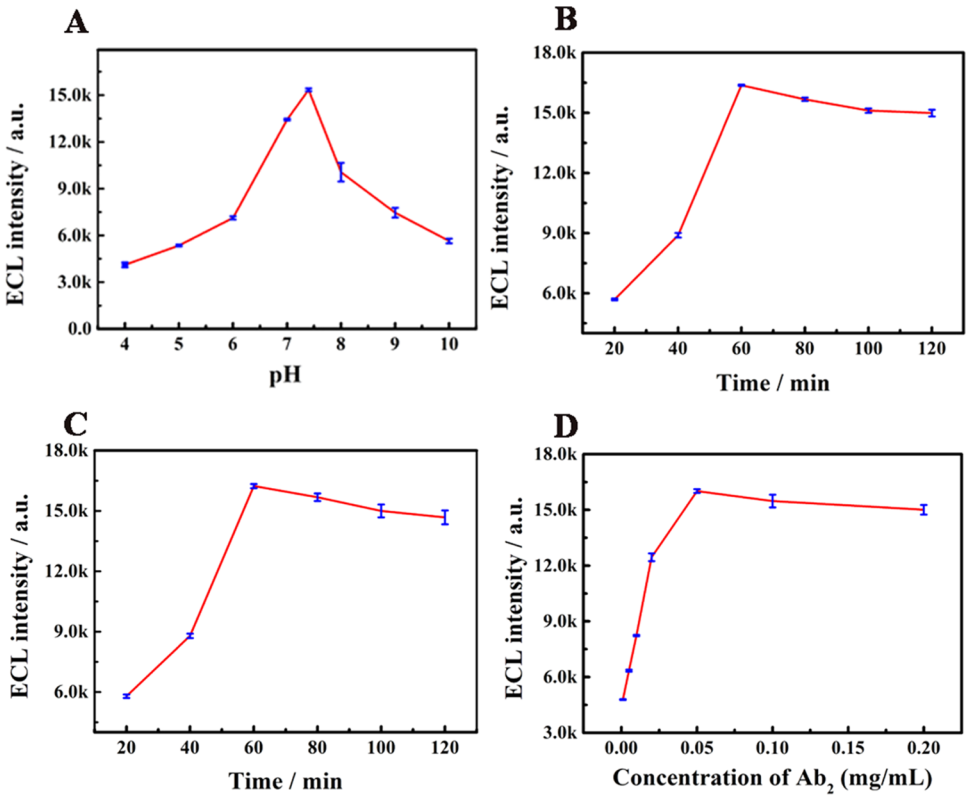

Figure 3. Effect of (A) pH of PBS, incubation time for (B) ncovNP and (C) Ab_2, and (D) concentration of Ab_2 on the ECL response at the biosensor incubated with 1.0 ng/mL ncovNP in PBS (3.0 mL, 0.10 M, pH 7.4). Scanning rate: 300 mV/s.

1978 a.u. (curve b). Nevertheless, the ECL signal strength of the biosensor with β-CD was about 9760 a.u., showing nearly fivefold enhancement than that without β-CD. It was demonstrated that our developed hydrophobic localized enrichment strategy of the co-reactant TDBA utilizing the hydrophobic cavity of β-CD could significantly enhance ECL emission and improve the detection sensitivity.

The electrochemical oxidation of co-reactant TDBA on different modified electrodes was explored using differential pulse voltammetry (DPV). First, the DPV profile in the case of TDBA being added to PBS was explored using the bare GCE, and the result is plotted in Figure 2E (curve a). A strong oxidation peak of TDBA was detected at +0.90 V, which was assigned to the production of $TDBA^{\bullet+}$ during the positive potential scanning. Subsequently, the DPV profile in the case of TDBA being immobilized by hydrophobic localized enrichment and covalent bonding was explored using TDBA-β-CD-Pt@Ab_2/ncovNP/Ab_1/PDP PNPs/GCE, and the result is plotted in Figure 2E (curve b), which shows a relatively strong oxidation peak at +0.90 V. Finally, the DPV profile with TDBA being immobilized only by covalent bonding (Pt−N bond) was also explored using TDBA-Pt@Ab_2/ncovNP/Ab_1/PDP PNPs/GCE, and the result is plotted in Figure 2E (curve c), which shows a dramatically decreased oxidation peak in the absence of β-CD. The above experiments confirmed that the hydrophobic cavity of β-CD could effectively enrich TDBA to produce more $TDBA^{\bullet+}$, thus improving ECL emission from PDP PNPs.

In addition, the electron paramagnetic resonance (EPR) was performed using 5,5-dimethyl-1-pyrroline N-oxide (DMPO) as TDBA radical scavenger to further confirm the hydrophobic localized enrichment of TDBA by β-CD. As seen from Figure 2F, under light irradiation, the EPR signal from the DMPO−TDBA adduct in the presence of β-CD is stronger than that

https://doi.org/10.1021/acs.analchem.1c05407
Anal. Chem. 2022, 94, 4446−4454

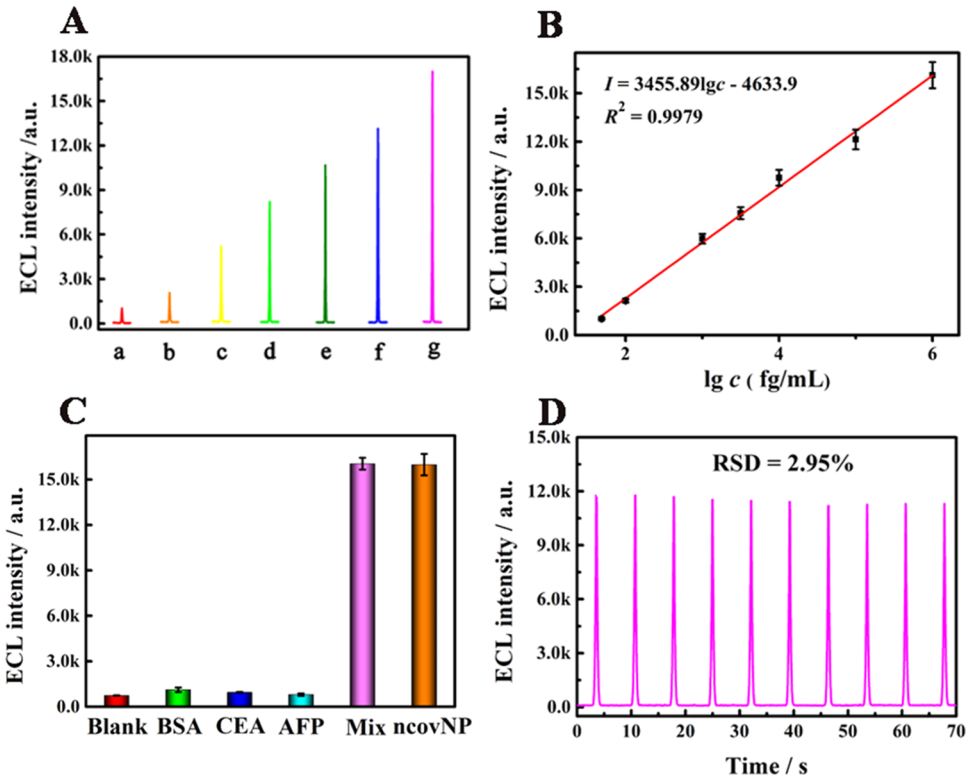

Figure 4. (A) ECL response of the biosensor TDBA-β-CD-Pt@Ab_2/ncovNP/Ab_1/PDP PNPs/GCE toward ncovNP (a) to (g): 50, 100 fg/mL, 1.0, 10, 100 pg/mL, 500 pg/mL, and 1.0 ng/mL. (B) Calibration curve for ncovNP detection. (C) ECL response to ncovNP (1 ng/mL) alone, blank sample, 100 ng/mL of interfering substance (BSA, CEA, and AFP) alone, and their mixtures in 3.0 mL of PBS (0.10 M, pH 7.4). (D) Stability of the biosensor with ncovNP (100 pg/mL). Scanning rate: 300 mV/s.

without β-CD, indicating that β-CD with an inner hydrophobic cavity could effectively enrich TDBA.

The possible ECL mechanism of the biosensor may be supposed as follows. First, the PDP PNPs and co-reactant TDBA were electro-oxidized to generate PDP $PNPs^{\bullet+}$ and $TDBA^{\bullet+}$, respectively. In the absence of β-CD (Scheme 2, without β-CD), less $TDBA^{+}$ would be produced when $TDBA^{\bullet}$ was immobilized only by covalent bonding (Pt—N bond), and then less $TDBA^{\cdot}$ would be produced through loss proton (H^{+}), thereby producing less excited species PDP PNPs*. Remarkably, in the presence of β-CD (Scheme 2, with β-CD), more $TDBA^{\bullet+}$ would be generated due to the hydrophobic interaction between TDBA and β-CD, and then $TDBA^{\bullet+}$ would lose H^{+} to produce more $TDBA^{\cdot}$, which further crashed with PDP $PNPs^{\bullet+}$ to form abundant PDP PNPs*, thus significantly promoting the ECL emission of the PDP PNPs/TDBA system.

Optimization of Experimental Conditions. Both cyclic voltammetry (CV) and electrochemical impedance spectroscopy (EIS) were applied to confirm the successful assembly of the biosensor (TDBA-β-CD-Pt@Ab_2/ncovNP/Ab_1/PDP PNPs/GCE), and Figure S5A,B plots the corresponding results, respectively. The corresponding discussions were described in the Supporting Information.

The optimization of experimental conditions is necessary for the analysis and application of the biosensor. In this work, the pH of PBS, the concentration of Ab_2, and the incubation time for ncovNP and Ab_2 were optimized using the biosensor TDBA-β-CD-Pt@Ab_2/ncovNP/Ab_1/PDP PNPs/GCE with 1.0 ng/mL ncovNP. Figure 3A plots the change of response signal with pH. It was observed that the ECL signal went up with increasing pH from 4.0 to 7.4, reaching its maximum at pH 7.4. The ECL intensity decreased gradually as pH exceeded 7.4. This phenomenon may be explained as the physiological pH is beneficial to the maintenance of bioactivity of the antibody and the antigen.

Figure 3B,C plots changes in response signal with the incubation time of ncovNP and Ab_2, respectively. As seen, the response signal gradually increased with the increasing incubation time and reached the maximum at 60 min. When the incubation time exceeded 60 min, the ECL intensity dropped slightly and gradually stabilized. Thus, the incubation time of 60 min was considered as the optimal incubation time for ncovNP and Ab_2 in this work.

Figure 3D plots the change in the response signal with the concentration of Ab_2. As seen, the ECL intensity increased as the concentration of Ab_2 ranged from 1.0 to 50 μg/mL. When the concentration exceeded 50 μg/mL, the ECL intensity decreased slightly and gradually stabilized. Thus, the concentration of 50 μg/mL was viewed as the optimizing concentration of Ab_2 in this work.

Furthermore, the amplification effects of different amines on the ECL emission of luminophore PDP PNPs were explored. The results are depicted in Figure S6 and the detailed discussions are presented in the **Supporting Information**. The results indicated that TDBA was an optimal co-reactant for PDP PNPs.

Analytical Performance of the Immunosensor. The application of ECL biosensor was first explored by quantitative bioassay of target ncovNP, and the results are plotted in Figure 4A,B. The ECL response in 3.0 mL of PBS (0.10 M, pH 7.4) gradually enlarged as the concentrations of ncovNP ranged

https://doi.org/10.1021/acs.analchem.1c05407
Anal. Chem. 2022, 94, 4446−4454

Table 1. Comparison of the Analytical Performance of Different ncovNP Detection Strategies

detection method	linear range	LOD	refs
immunochromatographic sensor	0.05−1.6 ng/mL	0.026 ng/mL	27
fluorescent immunoassay	0−120 ng/mL	0.33 ng/mL	28
voltammetric-based Immunosensor	100 ng/mL−1.0 pg/mL	0.4 pg/mL	29
half-strip lateral flow assay	0.53−0.77 ng/mL	0.65 ng/mL	30
electrochemical immunosensor	0.1 pg/mL−1 μg/mL	0.8 pg/mL	1
ECL immunosensor	50 fg/mL−1.0 ng/mL	22 fg/mL	this work

from 50 fg/mL to 1.0 ng/mL. Over this concentration range, the ECL intensity showed a good linear relationship with the logarithm of the concentration, and the detection limit as low as 22 fg/mL was obtained at the biosensor with a signal-to-noise ratio (S/N) of 3. The detailed calculation is presented in the Supporting Information. Compared to other works for ncovNP detection, the proposed ECL biosensor had a wider linear range and a lower detection limit. The comparison is depicted in Table 1.

The selectivity of the biosensor was further investigated in the case of BSA, carcinoembryonic antigen (CEA), and α-fetoprotein (AFP) as possible interfering substances. The ECL responses of the modified electrode toward target ncovNP (1.0 ng/mL), blank sample, selected interfering substance with a concentration of 100-fold ncovNP, and their mixtures were measured in 3.0 mL of PBS (0.10 M, pH 7.4). The results are shown in Figure 4C. As plotted, a strong ECL signal was observed in the case of ncovNP (1.0 ng/mL) alone and the mixtures containing ncovNP (1.0 ng/mL) and interfering substances. Moreover, the response was almost identical in both cases. Compared with the response toward ncovNP (1.0 ng/mL), the response to the interfering substances can be ignored, demonstrating good selectivity of the biosensor for ncovNP.

Stability is very important for the biosensor. The ECL signals at the biosensor incubated with 100 pg/mL ncovNP were recorded during 10 cycles of continuous potential scanning, and Figure 4D plots the results. As seen, the ECL response showed no significant change, and the relative standard deviation (RSD) of 2.95% was obtained, showing acceptable stability of the proposed ECL biosensor.

The reproducibility was also explored. The four biosensors constructed in the same batch and in different batches were used to perform the intra-assays and interassays in 3.0 mL of PBS (0.10 M, pH 7.4), respectively, and the results are shown in Figure S7. The RSDs in the intra-assays and interassays were 3.79 and 3.32%, respectively, demonstrating a favorable reproducibility of the proposed ECL biosensor.

Analysis of Real Serum Samples. To test the practicality of our constructed biosensors, recovery experiments were performed in serum using a standard addition method. The concentration of ncovNP in diluted serum with 50 fold was evaluated. Subsequently, ncovNP was added in three different concentrations in diluted serum to detect the recovery rates. As presented in Table S1, the recovery rates were in the range of 98.0−99.2%, indicating that the ECL platform was feasible for detecting ncovNP in real serum samples.

CONCLUSIONS

In this work, β-cyclodextrin (β-CD) with an inner hydrophobic cavity was innovatively developed to achieve a hydrophobic localized enrichment of co-reactant TDBA. Meanwhile, the coordination sites for metal ions of β-CD make it easy for Pt NPs to grow in situ on β-CD, which also could achieve the immobilization of TDBA via the Pt−N bond. The synergy of two forces, namely, hydrophobic localized enrichment and covalent bonding, resulted in a high loading of TDBA on the electrode surface. Meanwhile, the novel PDP PNPs with excellent ECL performance opened up a promising ECL polymer luminophore. The integration of the TDBA-β-CD-Pt nanocomposite and PDP PNPs achieved a sensitive detection of ncovNP, providing a new method for ncovNP. More importantly, β-CD shared with an inspiration in hydrophobic localized enrichment of co-reactants for improving the sensitivity of ECL detection.

ASSOCIATED CONTENT

Supporting Information

The Supporting Information is available free of charge at https://pubs.acs.org/doi/10.1021/acs.analchem.1c05407.

Reagents, materials, and apparatus; XPS spectrum of PDP PNPs and β-CD-Pt NPs (Figure S1); photophysical characterization of PDP PNPs (Figure S2); dispersion in water and luminescence stability of PDP PNPs (Figure S3); ECL response of PDP nanoparticles with and without PSMA (Figure S4); characterization of the assembly process of a biosensor (Figure S5); selectivity of co-reactants (Figure S6); reproducibility of the proposed biosensor for ncovNP (Figure S7); recovery rates of ncovNP in serum samples (Table S1); details of detection limit (PDF)

AUTHOR INFORMATION

Corresponding Author

Shihong Chen − *Key Laboratory of Luminescence Analysis and Molecular Sensing (Southwest University), Ministry of Education, College of Chemistry and Chemical Engineering, Southwest University, Chongqing 400715, P. R. China;* orcid.org/0000-0001-7101-1223; Phone: +86-23-68253172; Email: cshong@swu.edu.cn

Authors

Yingying Chen − *Key Laboratory of Luminescence Analysis and Molecular Sensing (Southwest University), Ministry of Education, College of Chemistry and Chemical Engineering, Southwest University, Chongqing 400715, P. R. China*

Ying He − *Key Laboratory of Luminescence Analysis and Molecular Sensing (Southwest University), Ministry of Education, College of Chemistry and Chemical Engineering, Southwest University, Chongqing 400715, P. R. China*

Jinwen Zhao − *Key Laboratory of Luminescence Analysis and Molecular Sensing (Southwest University), Ministry of Education, College of Chemistry and Chemical Engineering, Southwest University, Chongqing 400715, P. R. China*

Jin Zhang − *Chongqing Vocational Institute of Engineering, Chongqing 402260, P. R. China*

https://doi.org/10.1021/acs.analchem.1c05407
Anal. Chem. 2022, 94, 4446−4454

Ruo Yuan − *Key Laboratory of Luminescence Analysis and Molecular Sensing (Southwest University), Ministry of Education, College of Chemistry and Chemical Engineering, Southwest University, Chongqing 400715, P. R. China;* orcid.org/0000-0003-3664-6236

Complete contact information is available at: https://pubs.acs.org/10.1021/acs.analchem.1c05407

Notes

The authors declare no competing financial interest.

■ ACKNOWLEDGMENTS

This work was supported by the National Natural Science Foundation of China (21775122, 21775124, and 52172154), and the Natural Science Foundation of Chongqing City (cstc2020jcyj-msxmX0977 and cstc2018jcyjAX0693), China.

■ REFERENCES

(1) Eissa, S.; Zourob, M. *Anal. Chem.* **2021**, *93*, 1826−1833.
(2) Zhang, L. Y.; Fang, X. N.; Liu, X. B.; Ou, H. C.; Zhang, H. Y.; Wang, J. J.; Li, Q.; Cheng, H. Y.; Zhang, W. Y.; Luo, Z. F. *Chem. Commun.* **2020**, *56*, 10235−10238.
(3) Cai, Q. Y.; Mu, J. J.; Lei, Y.; Ge, J.; Aryee, A. A.; Zhang, X. G.; Li, Z. H. *Anal. Bioanal. Chem.* **2021**, *413*, 4645−4654.
(4) Haljasmägi, L.; Remm, A.; Rumm, A. P.; Krassohhina, E.; Sein, H.; Tamm, A.; Kisand, K.; Peterson, P. *Eur. J. Immunol.* **2020**, *50*, 1234−1236.
(5) Grant, B. D.; Anderson, C. E.; Williford, J. R.; Alonzo, L. F.; Glukhova, V. A.; Boyle, D. S.; Weigl, B. H.; Nichols, K. P. *Anal. Chem.* **2020**, *92*, 11305−11309.
(6) Li, J.; Lillehoj, P. B. *ACS Sens.* **2021**, *6*, 1270−1278.
(7) Hao, Q. X.; Xu, Q. Z.; Niu, S. Y.; Ding, C. F.; Luo, X. L. *Anal. Chem.* **2021**, *93*, 10679−10687.
(8) Guo, J. N.; Xie, M. S.; Du, P. Y.; Liu, Y.; Lu, X. Q. *Anal. Chem.* **2021**, *93*, 10619−10626.
(9) Yao, B.; Zhang, J.; Fan, Z. Q.; Ding, Y. D.; Zhou, B.; Yang, R. Y.; Zhao, J. F.; Zhang, K. *ACS Appl. Mater. Interfaces* **2021**, *13*, 19816−19824.
(10) Kim, H. Y.; Lee, J. H.; Kim, M. J.; Park, S. C.; Choi, M.; Lee, W.; Ku, K. B.; Kim, B. T.; Changkyun Park, E.; Kim, H. G.; Kim, S. I. *Biosens. Bioelectron.* **2021**, *175*, No. 112868.
(11) Amanat, F.; Stadlbauer, D.; Strohmeier, S.; Nguyen, T. H. O.; Chromikova, V.; McMahon, M.; Jiang, K.; Arunkumar, G. A.; Jurczyszak, D.; Polanco, J.; Bermudez-Gonzalez, M.; Kleiner, G.; Aydillo, T.; Miorin, L.; Fierer, D. S.; Lugo, L. A.; Kojic, E. M.; Stoever, J.; Liu, S. T. H.; Cunningham-Rundles, C.; Felgner, P. L.; Moran, T.; García-Sastre, A.; Caplivski, D.; Cheng, A. C.; Kedzierska, K.; Vapalahti, O.; Hepojoki, J. M.; Simon, V.; Krammer, F. *Nat. Med.* **2020**, *26*, 1033−1036.
(12) Wang, N. N.; Wang, Z. Y.; Chen, L. Z.; Chen, W. W.; Quan, Y. W.; Cheng, Y. X.; Ju, H. X. *Chem. Sci.* **2019**, *10*, 6815−6820.
(13) Wang, N. N.; Feng, Y. Q.; Wang, Y. W.; Ju, H. X.; Yan, F. *Anal Chem.* **2018**, *90*, 7708−7714.
(14) Liu, D.; Yang, G. M.; Zhang, X. L.; Chen, S. H.; Yuan, R. *Sens. Actuators, B* **2021**, *329*, No. 129210.
(15) Cui, L.; Zhou, J. H.; Li, C. C.; Deng, S. Y.; Gao, W. Q.; Zhang, X. M.; Luo, X. L.; Wang, X. L.; Zhang, C. Y. *ACS Appl. Mater. Interfaces* **2021**, *13*, 28782−28789.
(16) Feng, Y. Q.; Wang, N. N.; Ju, H. X. *Anal. Chem.* **2018**, *90*, 1202−1208.
(17) Wang, X. Y.; Xiao, S. Y.; Yang, C. P.; Hu, C. Y.; Wang, X.; Zhen, S. J.; Huang, C. Z.; Li, Y. F. *Anal. Chem.* **2021**, *93*, 14178−14186.
(18) Jiang, J. J.; Chen, D.; Du, X. Z. *Sens. Actuators, B* **2017**, *251*, 256−263.
(19) Zhou, Y.; Chen, S. H.; Luo, X. L.; Chai, Y. Q.; Yuan, R. *Anal. Chem.* **2018**, *90*, 10024−10030.
(20) Yuan, Y. L.; Gan, X. X.; Chai, Y. Q.; Yuan, R. *Biosens. Bioelectron.* **2014**, *55*, 313−317.
(21) Zeng, W. J.; Wang, K.; Liang, W. B.; Chai, Y. Q.; Yuan, R.; Zhuo, Y. *Chem. Sci.* **2020**, *11*, 5410.
(22) Yin, X. R.; Yang, P.; Zhang, H. M.; Zhu, Q. J.; Yuan, R.; Li, Y.; Liang, W. B. *Anal. Chem.* **2020**, *92*, 15120−15128.
(23) Dai, H.; Yang, C. P.; Ma, X. L.; Lin, Y. Y.; Chen, G. N. *Chem. Commun.* **2011**, *47*, 11915.
(24) Hanayama, H.; Yamada, J.; Tomotsuka, I.; Harano, K.; Nakamura, E. *J. Am. Chem. Soc.* **2021**, *143*, 5786−5792.
(25) Ma, H. M.; Li, X. J.; Yan, T.; Li, Y.; Liu, H. Y.; Zhang, Y.; Wu, D.; Du, B.; Wei, Q. *ACS Appl. Mater. Interfaces* **2016**, *8*, 10121−10127.
(26) Douhal, A. *Chem. Rev.* **2004**, *104*, 1955−1976.
(27) Liang, C. L.; Liu, B. C.; Li, J. F.; Lu, J. H.; Zhang, E. H.; Deng, Q. T.; Zhang, L.; Chen, R. A.; Fu, Y. S.; Li, C. Y.; Li, T. T. *Sens. Actuators, B* **2021**, *349*, No. 130718.
(28) Liu, J. H.; Ruan, G. T.; Ma, W. L.; Sun, Y. J.; Yu, H. D.; Xu, Z. H.; Yu, C. M.; Li, H.; Zhang, C. W.; Li, L. *Biosens. Bioelectron.* **2021**, No. 113823.
(29) Eissa, S.; Alhadrami, H. A.; Al-Mozaini, M.; Hassan, A. M.; Zourob, M. *Microchimica. Acta* **2021**, *188*, No. 199.
(30) Grant, B. D.; Anderson, C. E.; Williford, J. R.; Alonzo, L. F.; Glukhova, V. A.; Boyle, D. S.; Weigl, B. H.; Nichols, K. P. *Anal. Chem.* **2020**, *92*, 11305−11309.